QUARTERLY TECHNICAL PROGRESS REPORT
FOR THE PERIOD ENDING JUNE 30, 2007

TITLE: ANALYSIS OF CRITICAL PERMEABLITY, CAPILLARY PRESSURE AND ELECTRICAL PROPERTIES FOR MESAVERDE TIGHT GAS SANDSTONES FROM WESTERN U.S. BASINS

DOE Contract No. DE-FC26-05NT42660

Contractor:	University of Kansas Center for Research, Inc. 2385 Irving Hill Road Lawrence, KS 66044
DOE Program:	Natural Gas Technologies (Advanced Diagnostics & Imaging)
Award Date:	October 1, 2005
Total Project Budget:	$513,834
DOE Cost Amount:	$411,030
Program Period:	October 1, 2005 – September 30, 2007
Reporting Period:	April 1, 2007 – June 30, 2007
DOE Project Manager:	Purna Halder, NETL Tulsa, OK
Contractor Contact:	Alan P. Byrnes Kansas Geological Survey 1930 Constant Ave., Lawrence, Kansas 66047 email: abyrnes@kgs.ku.edu phone: 785-864-2177
Principal Investigators:	Alan P. Byrnes (Program Manager) Robert Cluff (Discovery Group) John Webb (Discovery group)

DISCLAIMER:

ABSTRACT:

Analysis of *in situ* mercury intrusion capillary pressure (MICP) for critical nonwetting phase saturation (S_{nwc}) was performed using both MICP inflection analysis and electrical resistance analysis on 70 samples. Analysis is progressing on additional samples. As measured by MICP curve inflection, average confined S_{nwc} = 0.028 ±0.046 for rocks with k_{ik} > 0.01 mD and average S_{nwc} = 0.048 ± 0.096 for rocks with $k_{ik} \leq$ 0.01 mD (error bars represent two standard deviations). As measured by increase in electrical resistance, average confined S_{nwc} = 0.043 ±0.11 for rocks with k_{ik} > 0.01 mD and average S_{nwc} = 0.078 ± 0.2 for rocks with $k_{ik} \leq$ 0.01 mD (error bars represent two standard deviations).

To date all 150 unconfined mercury intrusion capillary pressure (MICP) analyses are complete and 87 *in situ* (confined) MICP analyses are complete. Analysis is proceeding on the remaining *in situ* samples. Unconfined and *in situ* (confined) MICP analyses are compared for 73 matched sandstones cores. Between core plugs in a pair set several trends are evident. *In situ* and unconfined curves for high-permeability cores (k_{ik} > 1 mD) are nearly identical. With decreasing permeability the difference between unconfined and *in situ* threshold entry pressure increases. For all pairs this difference is greatest at the threshold entry pressure and decreases with decreasing wetting-phase saturation. At wetting phase saturations of 30-50% the *in situ* MICP curve crosses the unconfined curve and exhibits 0-5% lower wetting phase saturation with increasing capillary pressure. A good log-log correlation exists between the threshold entry pore size (and corresponding pressure or gas column height) and permeability or permeability/porosity. The slope of the relationship with k/ϕ (slope = 0.50) is statistically identical for both unconfined and confined conditions for correlation where permeability and porosity are referenced to the same confining stress conditions as the MICP analysis.

A combined oral and poster presentation is being presented at the Rocky Mountain Section meeting of the American Association of Petroleum Geologists at Snowbird, UT in October 6-9, 2007.

TABLE OF CONTENTS

LIST OF FIGURES

Acronyms

D = pore throat diameter (microns)
D_{te} = Threshold entry pore diameter (microns)
Hg = mercury
H_{te} = Threshold entry gas column height (ft)
k_{ik} = *in situ* Klinkenberg permeability, millidarcies
k_{mk} = geometric mean of *in situ* and routine Klinkenberg permeability (md)
md = mD = millidarcy, 1 md = 9.87×10^{-4} μm^2
MICP = mercury intrusion capillary pressure
Pc = capillary pressure (psia)
Pc_{res} = capillary pressure (psia) at reservoir conditions
Pc_{lab} = laboratory-measured capillary pressure (psia)
psia = pound per square inch absolute, 1 psi = 6.89 kPa = 0.00689 MPa
P_{te} = Threshold entry pressure (psia)
Snwc = critical nonwetting phase saturation
Snwi = initial nonwetting phase saturation
Snwr = residual nonwetting phase saturation
Swirr = "irreducible" wetting phase saturation
ϕ = porosity, percent or fraction depending on context
μ = interfacial tension (dyne/cm)
θ = contact angle (degrees)
^{o}F = temperature degrees Farenheit

INTRODUCTION

Objectives - Industry assessment of the regional gas resource, projection of future gas supply, and exploration programs require an understanding of the reservoir properties and accurate tools for formation evaluation of drilled wells. The goal of this project is to provide petrophysical formation evaluation tools related to relative permeability, capillary pressure, electrical properties and algorithm tools for wireline log analysis. Major aspects of the proposed study involve a series of tasks to measure drainage critical gas saturation, capillary pressure, electrical properties and how these change with basic properties such as porosity, permeability, and lithofacies for tight gas sandstones of the Mesaverde Group from six major Tight Gas Sandstone basins (Washakie, Uinta, Piceance, Upper Greater Green River, Sand Wash and Wind River). Critical gas saturation (Sgc) and ambient and *in situ* capillary pressure (Pc) will be performed on 150 rocks selected to represent the range of lithofacies, porosity and permeability in the Mesaverde.

Project Task Overview -

Task 1. Research Management Plan
Task 2. Technology Status Assessment
Task 3. Acquire Data and Materials
- Subtask 3.1. Compile published advanced properties data
- Subtask 3.2. Compile representative lithofacies core and logs from major basins
- Subtask 3.3. Acquire logs from sample wells and digitize

Task 4. Measure Rock Properties
- Subtask 4.1. Measure basic properties (k, ϕ, grain density) and select advanced population
- Subtask 4.2. Measure critical gas saturation
- Subtask 4.3. Measure in situ and routine capillary pressure
- Subtask 4.4. Measure electrical properties
- Subtask 4.5. Measure geologic and petrologic properties
- Subtask 4.6. Perform standard logs analysis

Task 5. Build Database and Web-based Rock Catalog
- Subtask 5.1. Compile published and measured data into Oracle database
- Subtask 5.2. Modify existing web-based software to provide GUI data access

Task 6. Analyze Wireline-log Signature and Analysis Algorithms
- Subtask 6.1. Compare log and core properties
- Subtask 6.2. Evaluate results and determine log-analysis algorithm inputs

Task 7. Simulate Scale-dependence of Relative Permeability
- Subtask 7.1. Construct basic bedform architecture simulation models
- Subtask 7.2. Perform numerical simulation of flow for basic bedform architectures

Task 8. Technology Transfer, Reporting, and Project Management
- Subtask 8.1 Technology Transfer
- Subtask 8.2. Reporting Requirements
- Subtask 8.3. Project Management

EXECUTIVE SUMMARY:

Analysis of *in situ* mercury intrusion capillary pressure (MICP) for critical nonwetting phase saturation (S_{nwc}) was performed using both MICP inflection analysis and electrical resistance analysis on 70 samples. Analysis is progressing on additional samples. As measured by MICP curve inflection, average confined S_{nwc} = 0.028 ±0.046 for rocks with k_{ik} > 0.01 mD and average S_{nwc} = 0.048 ± 0.096 for rocks with $k_{ik} \leq$ 0.01 mD (error bars represent two standard deviations). As measured by increase in electrical resistance, average confined S_{nwc} = 0.043 ±0.11 for rocks with k_{ik} > 0.01 mD and average S_{nwc} = 0.078 ± 0.2 for rocks with $k_{ik} \leq$ 0.01 mD (error bars represent two standard deviations).

To date all 150 unconfined mercury intrusion capillary pressure (MICP) analyses are complete and 87 *in situ* MICP analyses are complete. Analysis is proceeding on the remaining *in situ* samples. Unconfined and *in situ* (confined) MICP analyses are compared for 73 matched sandstones cores. Between core plugs in a pair set several trends are evident. *In situ* and unconfined curves for high-permeability cores (k_{ik} > 1 mD) are nearly identical. With decreasing permeability the difference between unconfined and *in situ* threshold entry pressure increases. For all pairs this difference is greatest at the threshold entry pressure and decreases with decreasing wetting-phase saturation. At wetting phase saturations of 30-50% the *in situ* MICP curve crosses the unconfined curve and exhibits 0-5% lower wetting phase saturation with increasing capillary pressure. A good log-log correlation exists between the threshold entry pore size (and corresponding pressure or gas column height) and permeability or permeability/porosity. The slope of the relationship with k/ϕ (slope = 0.50) is statistically identical for both unconfined and confined conditions for correlation where permeability and porosity are referenced to the same confining stress conditions as the MICP analysis.

A combined oral and poster presentation is being presented at the Rocky Mountain Section meeting of the American Association of Petroleum Geologists at Snowbird, UT in October 6-9, 2007.

RESULTS AND DISCUSSION:

TASK 4. MEASURE ROCK PROPERTIES

Subtask 4.3. Measure critical gas saturation

Analysis of *in situ* mercury intrusion capillary pressure (MICP) for critical nonwetting phase saturation was performed using both MICP inflection analysis and electrical resistance analysis on 70 samples. Analysis is progressing on additional samples. Each sample was subjected to step-wise, increasing, mercury-injection pressures ranging from 2 to 7,200 psi (0.01-50 MPa). To determine the critical non-wetting phase saturation, S_{nwc}, mercury intrusion analysis was performed on 2.54-cm diameter by 3-cm to 7-cm long cores hydrostatically confined at a pressure of 4,000 psi (27.6 MPa) greater than the mercury injection pressure, maintaining a net effective stress of 4,000 psi (27.6 MPa). Resistance across the core was measured using stainless steel electrodes on each end of the core (Figure 1). Sandstone matrix and evacuated pore space are both highly resistive and the clean, dry, evacuated sandstone samples investigated all exhibited resistance ranging from 0.15-4 x 10^6 ohms (ohms). At the critical saturation of the percolation threshold, with formation of a continuous mercury tendril across the sample, resistance across the core decreases abruptly by one-third to five orders of magnitude. From each sample's capillary pressure curve the saturation associated with the characteristic length, l_c, as defined by Thompson et al. (1987), was measured at the first inflection point. Uncertainty in the

determination of the mercury saturation associated with the inflection point is estimated to be S_{nwc} $\pm$0.01 to $\pm$0.005 depending on the injection curve profile. Figure 2 illustrates the relationship between S_{nwc} and permeability, as measured by the inflection point and electrical resistance on the 70 confined MICP samples. As measured by MICP curve inflection, average confined S_{nwc} = 0.028 ±0.046 for rocks with k_{ik} > 0.01 mD and average S_{nwc} = 0.048 ± 0.096 for rocks with $k_{ik} \leq$ 0.01 mD (error bars represent two standard deviations). As measured by increase in electrical resistance, average confined S_{nwc} = 0.043 ±0.11 for rocks with k_{ik} > 0.01 mD and average S_{nwc} = 0.078 ± 0.2 for rocks with $k_{ik} \leq$ 0.01 mD (error bars represent two standard deviations).

For 43% of the samples, the inflection-interpreted S_{nwc} corresponds to the mercury saturation (S_{Hg}) above which electrical resistance across the core exhibits values greater than 0.15-4 x 10^6 ohms and below which resistance values are less than 5-50 ohm, a decrease of more than four- to six-orders of magnitude. This is interpreted to result from formation of a highly-conductive continuous path of mercury through the sample. For an additional 25% of the samples the interpreted S_{nwc} corresponded to a decrease in resistance of greater than 1.5 standard deviations of the average of the previous five resistance measurements, interpreted to result from formation of a continuous mercury path of limited volume and high tortuosity. From these results, for 68% of the samples the inflection and the resistance measurements can be interpreted to agree on the interpreted critical saturation. Within this population, average S_{nwc} = 0.036$\pm$0.08 with a maximum value of S_{nwc} = 0.175. The remaining 32% of samples did not exhibit a resistance decrease until mercury saturation increased an additional S_{Hg}= 0.03-0.29 (average S_{Hg} = 0.13), corresponding to mercury saturations of S_{Hg}= 0.02-0.42 (average S_{Hg} = 0.16). For these 32% of samples the inflection S_{nwc} is interpreted to represent "pretender" clusters in a series network and the resistance-interpreted S_{nwc} provides a measure of the sample-spanning S_{nwc}.

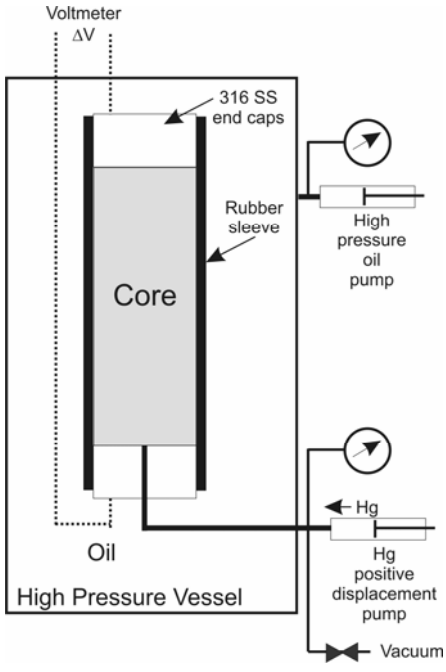

Figure 1. Schematic of high-pressure, mercury-intrusion and electrical-resistance instrument. Samples were confined at a pressure of 4,000 psi (27.6 MPa) greater than the mercury-injection pressure for all pressures.

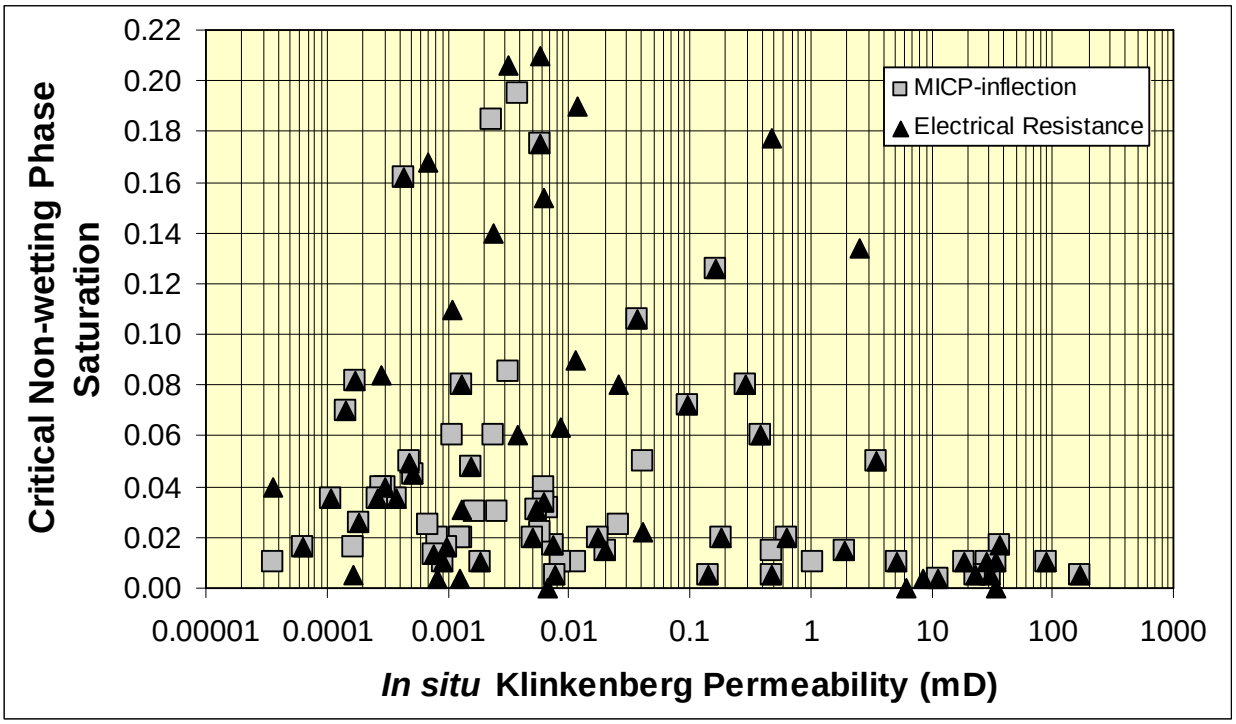

Figure 2. Crossplot of critical mercury (nonwetting) saturation forming a sample spanning cluster as measured by MICP curve inflection (gray squares) and change in electrical resistance (black triangles) for 70 Mesaverde sandstone samples.

Subtask 4.3. Measure *in situ* and routine capillary pressure

Unconfined and *in situ* (confined) mercury intrusion capillary pressure (MICP) analyses are compared for 73 matched sandstones cores. Two matched core plugs were obtained by cutting a single long core plugs into two plugs of 3-5 cm in length. On both plugs porosity and permeability were measured. Statistics for 630 adjacent core plug pairs have been discussed in the December 31, 2006 Quarterly Report. From a total population of greater than 700 core plug pairs, a population of 150 core plugs pairs was selected for unconfined and *in situ* (confined) MICP analysis. These sample pairs exhibit an average porosity difference between plug pairs of 0.15+0.3 porosity units (1.8%+3.6% of the average pair porosity) and within a factor of 1.4$\underline{+}$2.8 for the *in situ* Klinkenberg permeability (within an average factor of 1.13$\underline{+}$2.5 of the average k_{ik}). Each sample was subjected to step-wise, increasing, mercury-injection pressures ranging from 2 to 9,300 psi (0.01-64.1 MPa) for unconfined and 2 to 7,200 psi (0.01 – 50 MPa) for confined. For *in situ* MICP cores were hydrostatically confined at a pressure of 4,000 psi (27.6 MPa) greater than the mercury injection pressure, maintaining a net effective stress of 4, 000 psi (27.6 MPa). For these analyses the *in situ* pore volume was calculated using previously reported compressibility relations and the pore volume measured by routine helium porosity. To date all unconfined analyses are complete and 87 *in situ* MICP analyses are complete. In the present analysis the threshold entry pressure of 70 samples and curve shapes are compared. Analysis is proceeding on the remaining *in situ* samples.

Figure 3 illustrates example unconfined and *in situ* MICP curves for pairs of high- to low-permeability from different wells and basins. Comparison among pairs shows that threshold entry pressures increase with decreasing permeability. Between core plugs in a pair set several trends are evident. *In situ* and unconfined curves for high-permeability cores (k_{ik} > 1 mD) are

nearly identical. With decreasing permeability the difference between unconfined and *in situ* threshold entry pressure increases. For all pairs this difference is greatest at the threshold entry pressure and decreases with decreasing wetting-phase saturation. At wetting phase saturations of 30-50% the *in situ* MICP curve crosses the unconfined curve and exhibits 0-5% lower wetting phase saturation with increasing capillary pressure. MICP curve data are still being analyzed but it can be interpreted that confining stress exerts principal influence on the largest pore throats and that pore throats accessed at non-wetting phase saturations below approximately 50% are not significantly affected by confining stress. This is consistent with these smaller pores comprising pore space within pore bodies or in regions of the rocks where stress is not concentrated.

Laboratory air-mercury capillary pressure data were converted to reservoir gas-brine capillary pressure data using the standard equation (Purcell, 1949):

$$Pc_{res} = Pc_{lab} (\sigma\cos\theta_{res}/\sigma\cos\theta_{lab}) \quad (1)$$

where Pc_{res} is the gas-brine capillary pressure (psia) at reservoir conditions, Pc_{lab} is the laboratory-measured capillary pressure (psia), $\sigma\cos\theta_{res}$ is the interfacial tension (σ, dyne/cm) times the cosine of the contact angle (θ, degrees) at reservoir conditions, and $\sigma\cos\theta_{lab}$ is the interfacial tension times the cosine of the contact angle at laboratory conditions. For air-mercury capillary pressure measurements an air-mercury interfacial tension of 484 dyne/cm and a contact angle of 140 degrees was assumed. To determine the water saturation in any given rock as a function of height above the free-water level, it is necessary to convert the capillary pressure data to height above free-water level. This conversion was performed using the standard relation (Hubbert, 1953):

$$H = Pc_{res}/(E(\rho_{brine}-\rho_{gas})) \quad (2)$$

where H is the height (ft) above free-water level, Pc_{res} is the capillary pressure (psia) at reservoir conditions, ρ_{brine} and ρ_{gas} are the density of brine and gas at reservoir conditions and E is a constant (0.433(psia/ft)/(g/cc)) for converting density to pressure gradient.

From the air-mercury capillary pressure data, pore-throat diameter was calculated using the modified Washburn (1921) relation:

$$D = 4F\sigma\cos\theta/Pc \quad (3)$$

where Pc = capillary pressure (psia), F = 0.145 ((psia·cm·μm)/dyne), θ = contact angle (140 degrees), σ = interfacial tension (484 dyne/cm), and D = pore-throat diameter (μm, microns). This relation assumes that the nonwetting phase (i.e., gas) enters the pores through circular pore throats.

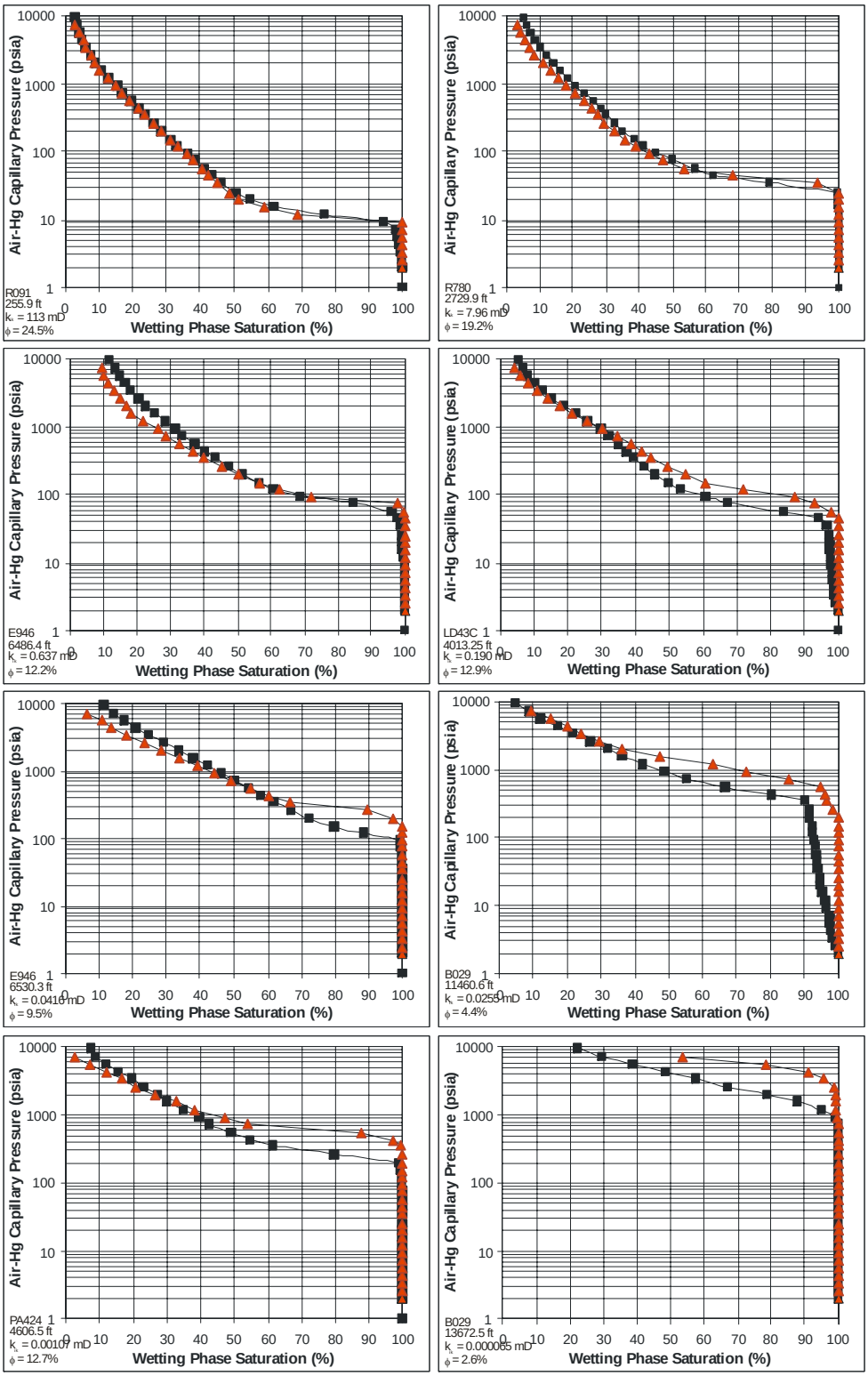

Figure 3. Examples of *in situ* (red triangles) and unconfined (black squares) air-mercury capillary pressure curves. Threshold entry pressure for samples under *in situ* conditions are greater than for unconfined conditions with the difference in pressure increasing with decreasing permeability. At higher pressures curves frequently cross. Trends are similar to those reported by Byrnes and Keighin (1993).

Variables in equations 1 to 3 that change with reservoir pressure, temperature, gas chemistry, and brine chemistry include σ, ρ_{brine}, and ρ_{gas}. To convert laboratory properties to reservoir properties for use in the equations above the range of Mesaverde reservoir conditions were defined as; 1) reservoir pressures - 2,500-13,000 psia; 2) temperatures- 90-260 ^{o}F, 3) gas gravity - 0.55-0.70, and 4) brine density -1.01-1.11 grams/cubic centimeter (g/cc). For the range in temperature, methane-water interfacial tension (IFT) ranges from 33-58 dyne/cm and for intermediate conditions of 168 ^{o}F can be considered to be 47$\pm$12 dyne/cm using methane-brine interfacial tension values reported by Jennings and Newman (1971). For the range in pressure, temperature, and gas gravity, and reasonable combinations of these variables to represent reservoir conditions, gas density (ρ_{gas}) at reservoir conditions ranges from approximately 0.12-0.36 g/cc with an intermediate value of 0.24$\pm$0.12 g/cc and the corresponding gas pressure gradient equals 0.104$\pm$0.052 psi/ft. Using $\sigma\cos\theta_{res}$ = 47$\pm$12 dyne/cm, $\sigma\cos\theta_{lab}$= 370.8 dyne/cm, ρ_{gas} = 0.24$\pm$0.12 g/cc, and ρ_{brine} = 1.06$\pm$0.05 g/cc, MICP pressures can be transformed into equivalent height above free water using Equation 2.

Figure 4 illustrates the relationship between MICP-measured threshold entry pressure and the ratio of Klinkenberg permeability/porosity. It also shows the equivalent relationships for threshold entry pore diameter and threshold entry gas column height calculated using equations 1 through 3.

Data are presented for both unconfined and *in situ* MICP measurements. Several details concerning the variables plotted are important to note. The abscissa in Figure 4 represents two different ratios; the unconfined and *in situ* data. For the *in situ* data the abscissa represents k_{ik}/ϕ_i, the ratio of the *in situ* Klinkenberg permeability and the *in situ* porosity (calculated from the routine helium porosity corrected for compression to *in situ* conditions using equations presented in the March 31, 2007 Quarterly Report). The MICP equipment used does not provide direct measurement of the sample pore volume under confining stress thus empirical correction of unconfined measured pore volume using helium to confined stress conditions is required. This empirical correction introduces uncertainty of approximately $\pm$0-3.5% (1 std. dev.) into the *in situ* pore volume, varying with saturation, that translates to a possible error in wetting phase saturation of up to $\pm$0-3.5% (1 std dev). Error increases with decreasing wetting phase saturation and "irreducible" saturation is the most affected.

The compressible nature and the threshold entry pressure of these rocks also results in uncertainty for standard unconfined MICP. Up to the threshold entry pressure mercury has not entered the sample and mercury both surrounds the sample and compresses the sample hydrostatically. For sandstones with permeability greater than 0.2 mD the threshold entry pressure of mercury is less than 100 psi (700 kPa) and corresponding pore volume compression is less than 1%. However, with decreasing permeability the threshold entry pressure and resulting confining stress increases (Figure 5) and pore volume decreases. For low-permeability sandstones with k_{ik} < 0.001 mD, confining stress exceeds 1,000 psi (7 MPa) and pore volume is correspondingly an average of 3.5% less than unconfined conditions. As mercury enters the sample pore volume it increases the pore pressure of the fraction of the pore volume occupied and decreases the net effective stress for portions of the sample while uninvaded portions of the rock sample remain compressed. With step-wise increase in injection pressure and confining stress for uninvaded rock volume the net effective stress on the uninvaded rock continually changes while invaded portions are decompressed. Comparison of saturations calculated using the unconfined pore volume and pore volume corrected for mercury-induced confining stress are being analyzed.

For the unconfined data the abscissa represents k_{mk}/ϕ_a, the ratio of the geometric mean of the routine Klinkenberg permeability, measured under "routine" conditions of 600 psi (4.1 MPa) confining stress, and the *in situ* Klinkenberg permeability, measured under 4,000 psi (27.6 MPa) confining stress, divided by the unconfined routine helium porosity, ϕ_a. The mean permeability and not the routine Klinkenberg permeability is used because; 1) the lower-permeability rocks are under confining stress by surrounding mercury at the threshold entry pressure, and 2) for all samples routine and *in situ* permeabilities were measured prior to MICP resulting in permeability hysteresis. *In situ* permeability was measured at 4,000 psi confining stress. When this confining stress was released the permeability of most samples does not return immediately to the routine permeability but instead exhibits permeability hysteresis and time-dependent change of routine permeability. The permeability that most closely corresponds to the stress conditions of the unconfined MICP is a Klinkenberg permeability measured at the threshold entry pressure (P_{te}) measured immediately prior to MICP analysis. This permeability is intermediate between the initially measured routine and *in situ* Klinkenberg permeabilities. Klinkenberg permeability at this precise stress condition was not measured and the mean Klinkenberg permeability represents a value that is closer to this condition than either the routine or *in situ* values. Figure 5 illustrates the relationship between unconfined P_{te} and routine, *in situ* and mean permeabilities and shows that the mean permeability exhibits the same relationship as the *in situ* MICP for which these stress issues do not exist.

Figure 4 illustrates the good correlation between the threshold entry pore size (and corresponding pressure or gas column height) and permeability. The slope of this relationship is statistically identical for both unconfined and confined conditions because the abscissa represents each set of conditions. Unconfined samples exhibited higher permeabilities and larger threshold entry pore diameters. With application of confining stress the permeability decreased due to the decrease in pore throat diameter. The slope of the relationship between pore size and permeability, 0.5, is the same as the scaling parameter proposed by Leverett (1941) who proposed normalizing capillary pressure using $(k/\phi)^{0.5}$. Because permeability is well correlated with threshold pore throat size it can be used to correct unconfined capillary pressure curves to *in situ* conditions.

Permeability shows little dependence on confining stress for high-permeability rocks ($k > 1$ md) because confining stress induces little change in pore throat size. The influence of confining stress on permeability increases with decreasing permeability. Figures 3 through 5 show that confining stress has little influence on pore size or capillary pressure in the higher-permeability rocks and the influence increases with decreasing rock permeability. Although permeability is treated as the independent variable because it is a convenient variable to measure, and is the abscissa in Figures 3-5, permeability is actually the dependent variable and pore size, and its change with confining stress, is the independent variable.

The results presented here indicate that capillary pressure measurements on low-permeability sandstones are significantly influenced by confining stress, consistent with observed permeability changes.

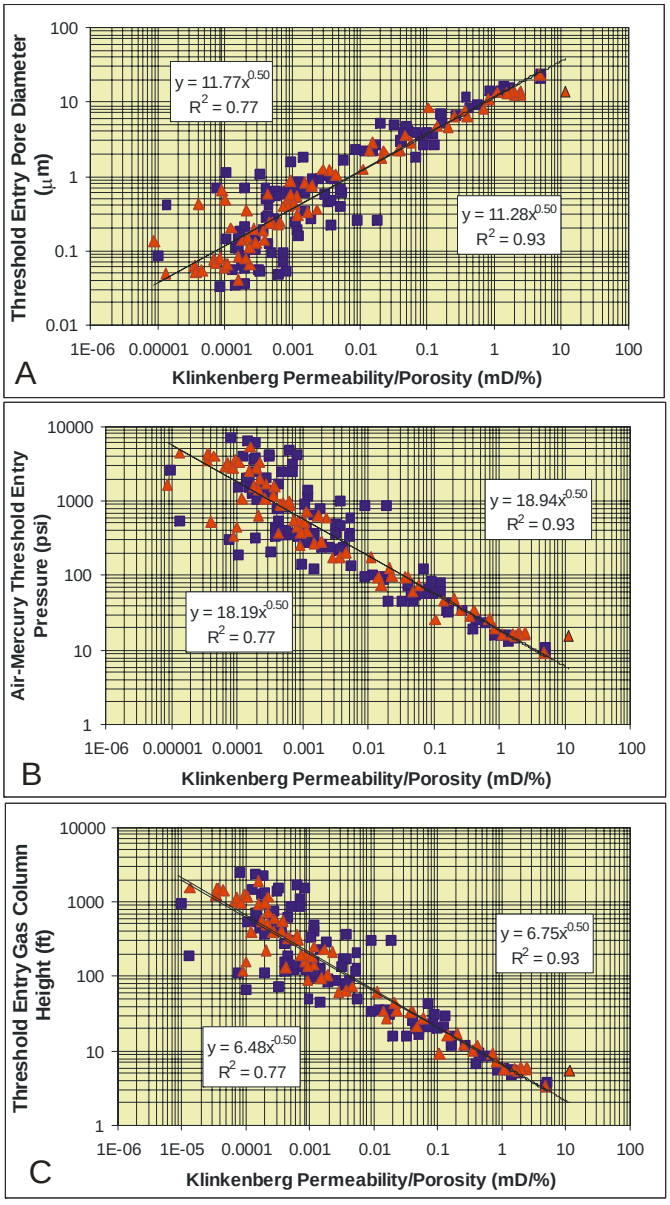

Figure 4. Crossplot of threshold entry pore diameter (A), air-Hg pressure (B), and gas column height (C), measured by MICP and calculated using equations 1-3 in text, versus the ratio of k_{ik}/ϕ_i for *in situ* data (red triangles), and k_{mk}/ϕ_a for unconfined data (blue squares). Variables and stress conditions are discussed in the text.

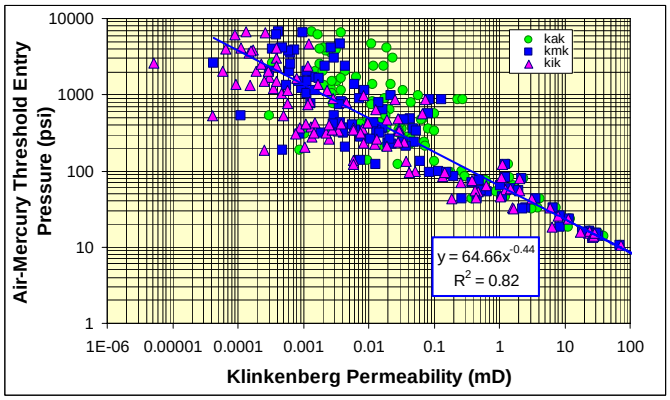

Figure 5. Crossplot of air-mercury threshold entry pressure versus the routine Klinkenberg permeability (green circles), measured at 600 psi confining stress, *in situ* Klinkenberg permeability (magenta triangles), measured at 4,000 psi confining stress, and the geometric mean of these permeabilities (blue squares).

TASK 8. TECHNOLOGY TRANSFER, REPORTING, PROJECT MANAGEMENT

Subtask 8.1 Technology Transfer

A combined oral and poster presentation is being presented at the Rocky Mountain Section meeting of the American Association of Petroleum Geologists at Snowbird, UT in October 6-9, 2007. The presentations will present results of Mesaverde properties measured. In addition, residual saturation measurements sand trends were used to interpret properties of the Ericson and a talk is presented on this subject. Abstracts follow:

Regional petrophysical properties of Mesaverde low-permeability sandstones

Alan P. Byrnes, Kansas Geological Survey, Kansas
John Webb, The Discovery Group Inc., Denver, Colorado
Robert M. Cluff, The Discovery Group Inc., Denver, Colorado

Petrophysical properties of Mesaverde Group tight gas sandstones for the range of lithofacies present in the Washakie, Uinta, Piceance, Upper Greater Green River, Wind River, and Powder River basins exhibit consistent trends among lithofacies. Grain density for 2400 samples averages 2.654±0.033 g/cc (±1sd) with grain density distributions differing slightly among basins. The Klinkenberg gas slip proportionality constant, b, can be approximated using the relation: $b(atm) = 0.851\ k_{ik}^{-0.34}$. Regression provides a relation for *in situ* Klinkenberg permeability (k_{ik}): $\log k_{ik} = 0.282\ \phi_i + 0.18\ RC2 - 5.13$ (±4.5X,1 sd), where ϕ_i = *in situ* porosity, and RC2 = a size-sorting index. Artificial neural network analysis provides prediction within ±3.3X. Analysis of 700 paired samples indicates 90% of all samples exhibit porosity within 10%-20%. Permeability exhibits up to 40% variance from a mean value for 80% of samples.

Capillary pressure (Pc) exhibits an air-mercury threshold entry pressure (P_{te}) versus k_{ik} trend of $P_{te} = 30.27\ k_{ik}^{-0.44}$ and wetting-phase saturation at any given Pc (for 350< Pc < 3350 psia air-Hg) and k_{ik} of $S_w = A\ k_{ik}^{-0.138}$ where $A = -13.1*\ln(Pc_{air\text{-}Hg})+117$. Accuracy of the Leverett J function is poorer. Hysteresis Pc analysis indicates that residual nonwetting-phase saturation to imbibition (*Srnw*) increases with increasing initial nonwetting phase saturation (*Snwi*) consistent with the Land-type relation: 1/Snwr-1/Snwi = 0.8±0.2. Electrical resistivity measurements show that the Archie cementation exponent (*m*) decreases with decreasing porosity (ϕ) below approximately 6% and can be generally described by the empirical relationship: $m = 0.95\text{-}0.092\ \phi + 0.635\ \phi^{0.5}$. These relationships are still being investigated. The Mesaverde Project website is (http://www.kgs.ku.edu/mesaverde).

What's the matter with the Ericson?

Robert M. Cluff, The Discovery Group Inc., Denver, Colorado
Keith W. Shanley, The Discovery Group Inc., Denver, Colorado
Alan P. Byrnes, Kansas Geological Survey, Lawrence, Kansas
and John W. Robinson, North Ranch Resources, Littleton, Colorado

The Cretaceous Ericson Formation is a clean, quartzose, blanket-like sandstone that underlies the prolific gas productive Almond Formation across the entire Washakie basin. The top several tens of feet of the Ericson are penetrated by most wells drilled to the Almond in order to obtain sufficient rathole for logging the entire Almond. Thus there are thousands of Ericson tests, most of which show one or more indications of gas pay in the Ericson. These include 6-11% porosity, resistivity >50 ohm-m, neutron-density gas cross-over, and mudlog shows. Archie saturation calculations using appropriate R*w* values almost universally indicate "gas pay" comparable to overlying Almond sands. And yet, nearly all attempts at completions in the Ericson result in extremely high water volumes with minor amounts of gas, typically <250 MCFD. Commercial production has only been found over large structural closures, such as Canyon Creek Field, or in very small areas of a few wells on regional dip.

Our interpretation is the Ericson displays all the characteristics of a watered out gas reservoir. Log and mudlog gas shows are probably real, and calculated Archie saturations are approximately correct. Completion attempts demonstrate the Ericson is at or near residual gas saturation (S*gr*), with high relative permeability to water and low relative permeability to gas. Consequently the Ericson appears to have formerly been a widespread gas reservoir, perhaps filled over most of the central Washakie basin in the early Tertiary, but with late Tertiary uplift and structural re-adjustment of the Wamsutter Arch gas spilled laterally to the east and west leaving a residual gas column behind. The stratigraphic continuity of the Ericson and high net:gross offers little in the way of internal trapping opportunities, so producible gas only occurs in local stratigraphic traps and over structural closures. The remaining enigma was the very high S*gr*, by our calculations 40 to 60% in most wells, which we find to be fully consistent with recently determined imbibition capillary pressure behavior in tight sandstones.

What's the matter with the Ericson is that it has leaked it's gas charge, and what was left behind is not producible. Clearly gas charge is widespread and there is sufficient reservoir quality for the sands to produce, so exploration efforts should focus on structural closures, subtle fault traps, or large stratigraphic pinchouts. Minor producible accumulations will continue to be found by serendipity, but they will be difficult to recognize because S*gr* is so high and is close to initial saturation conditions.

CONCLUSIONS

Analysis of *in situ* mercury intrusion capillary pressure (MICP) indicates that for the samples analyzed critical nonwetting phase saturation (S_{nwc}) varies from 0-0.08$\pm$0.02 and increases slightly with decreasing permeability. These low Snwc values are consistent with low critical gas saturation values of < 0.10 reported in the literature for sandstones and low-permeability sandstones. It is important to note that the cores analyzed do not represent permeability heterogeneities in series, which has been shown from network analysis to increase critical nonwetting phase saturation.

In situ and unconfined curves for high-permeability cores (k_{ik} > 1 mD) are nearly identical. With decreasing permeability the difference between unconfined and *in situ* threshold entry pressure increases. For all pairs this difference is greatest at the threshold entry pressure and decreases with decreasing wetting-phase saturation. At wetting phase saturations of 30-50% the *in situ* MICP curve crosses the unconfined curve and exhibits 0-5% lower wetting phase saturation with increasing capillary pressure. A good log-log correlation exists between the threshold entry pore size (and corresponding pressure or gas column height) and permeability or permeability/porosity. These results indicate that the significant permeability decrease characteristic of low-permeability sandstones is caused by a decrease in pore throat size and primarily the threshold entry and largest pore throat sizes.

Confined mercury capillary pressure measurements are preceding smoothly but slowly because equilibration times are longer than previously estimated for the lowest-permeability samples. Because of analysis times of greater than 1 day per sample scheduling for this analysis is behind the timetable presented in the Management Plan. Analysis is being performed within the approved budget.

REFERENCES

Byrnes, A.P., and Keighin, C.W., 1993, Effect of confining stress on pore throats and capillary pressure measurements for selected sandstone reservoir rocks; Proceedings American Association of Petroleum Geologists Annual Convention, April 25-28, New Orleans, LA, p. 82.

Hubbert, M. K., 1953, Entrapment of petroleum under hydrodynamic conditions: AAPG Bulletin, v. 37, p. 1954-2026.

Jennings, H.Y., Jr., and G.H. Newman, 1971, The effect of temperature and pressure on the interfacial tension of water against methane-normal decane mixtures, Trans. AIME, v. 251, p. 171-175.

Leverett, M.C., 1941,Capillary behavior in porous solids, AIME Trans. V. 142 (1941) p. 152–169.

Purcell, W. R., 1949, Capillary pressure – their measurements using mercury and the calculation of permeability therefrom: American Institute of Mechanical Engineers Petroleum Transactions, v. 186, p. 39-48.

Thompson, A.H., A.J. Katz, and R.A. Raschke, 1987, Mercury injection in porous media: a resistance Devil's staircase with percolation geometry, Physical Review Letters, v. 58, no. 1, p. 29-32.

Washburn, E. W., 1921, A method of determining the distribution of pore sizes in a porous material: Proceedings of the National Academy of Sciences, v. 7, p**.** 115-116.